along the needle-shaped crystal axis have been shown to increase during storage for 2–7 days under dry and humid conditions, and regular triangular or rectangular features have been observed, indicating surface recrystallization of caffeine cocrystals. Changes in the surface topology of spray-dried lactose particles have also been observed by AFM.[8] Linear striated features due to crystallization appeared and gradually propagated across the surface of the particles stored at 58% relative humidity. The crystallized surface had an irregular topology with a well-ordered and definable structure over relatively small areas but not over wide areas, suggesting that secondary nucleation and growth had occurred. Furthermore, the surface crystallization rate of spray-dried amorphous lactose has been reported.[9,10] Images of rectangular shapes on the surface of the lactose particles have been sequentially captured as a function of time by AFM, and the growth rate has been estimated from the time profiles of width and length of the rectangular shapes.

The aim of this study was to investigate the feasibility of AFM for determining crystal growth rates at the surface of amorphous NFD in the presence and absence of polymer excipients by capturing sequential images in specific areas of the samples. The polymer excipients used were polyethylene glycol (PEG) and α,β-poly(N-5-hydroxypentyl)-L-aspartamide (PHPA). PEG is one of the typical polymers used for preparation of solid dispersions to improve drug dissolution.[11–13] PHPA has been selected as a model of a partially immiscible polymer with NFD[14] because the miscibility of an amorphous drug with polymer excipients is one of the factors that determine the physical stability of amorphous solid dispersions.[15] Here, we compared the growth rates estimated from AFM measurements with the values estimated from polarized light microscopy measurements. Spatial information on the crystallization of NFD alone and that in these solid dispersions obtained by AFM is described.

EXPERIMENTAL

Materials and Sample Preparation

Nifedipine was obtained from Sigma–Aldrich Company (St. Louis, MO). PEG with an average molecular weight of 300 was purchased from Wako Pure Chemical Industries Ltd. (Osaka, Japan). PHPA was synthesized via polycondensation of L-aspartic acid and 1-aminopentane using a method similar to that reported previously.[16]

The sample of amorphous NFD was prepared on a glass plate as follows: Crystalline NFD (approximately 20 mg) was put on a glass plate (thickness 0.12–0.17 mm, diameter 18 mm), and the plate was placed in a differential scanning calorimeter (DSC2920; TA Instruments, New Castle, DE) at 190°C for approximately 2 min under dry nitrogen flow (30 mL/min). Then, the glass plate was removed from the differential scanning calorimeter and cooled to room temperature on a stainless steel block for several seconds. The samples were stored in a desiccator over phosphorous pentoxide to avoid moisture, and were kept at 25°C before AFM measurements. Amorphous NFD samples containing PEG or PHPA were prepared as described above using approximately 20 mg of NFD–polymer mixtures, which were obtained by solvent evaporation of NFD–PEG methanol solution and NFD–PHPA ethanol solution.

Amorphous NFD containing PEG was also prepared in a glass Petri dish (inner diameter 23 mm, depth 7 mm) to visually examine positions of NFD crystallization in the NFD–PEG solid dispersion. Approximately 2 g of NFD–PEG (5%) mixture in the Petri dish was kept at 197°C for 5 min in an oven, and then quenched on a stainless steel block that had been precooled with ice.

AFM Measurements

Atomic force microscopy (Dimension 3100; Veeco Instruments, Plainview, NY) measurements were performed in tapping mode, analogous to noncontact mode and alternating current mode, under ambient temperature (26±1°C) and relative humidity (<50%). The operation software used was Nanoscope 5.30r1 (Veeco Instruments). Silicon probes with a nominal spring constant of 42 N/m and a nominal length of 125 μm were used. AFM images were collected at a scan speed of 50–150 μm/s for a square region of 50–100 μm with 256–512 collecting points per line. The topography images were collected by scanning the probe across the surface of the sample in a raster pattern, line by line, from one side of the square area toward the opposing side. Because the scan direction changed alternately from downward and upward during sequential data collection, only the images collected in the downward scan direction were used to determine the crystal growth rate. To investigate the potential effects of physical stimulation from the AFM probe on the crystal growth rate of NFD, AFM images were collected at various time intervals (1.3–17 min/image) by varying the scan range, scan speed, and collecting points per line.

Measurements of Crystal Growth Rate by Polarized Light Microscopy

Crystal growth rates of NFD in amorphous NFD alone and NFD–polymer solid dispersions were determined using a polarized light microscope (ECLIPSE E600 POL; Nikon Corporation, Tokyo, Japan) with a ×10 objective lens (depth of field 8.46 μm). The microscope was equipped with a heating/cooling

 DOI 10.1002/jps

stage (THMS600; Linkam Scientific Instruments, Tadworth, Surrey, UK) to control the temperature of the sample. The sample of amorphous NFD, prepared as described above, was placed in the chamber of the heating/cooling stage, which had been preheated to 25°C. Then, the chamber was purged with dry nitrogen gas for 5–10 min to remove moisture, and hermetically closed. The focus of the microscope was adjusted to the free surface of the amorphous sample, and the crystal growth was observed. Microscopy images were recorded at constant time intervals by a digital camera (DXM1200F; Nikon Corporation) attached to the microscope, and were analyzed using Lumina Vision software (Mitani Company, Fukui, Japan). The crystal growth rates were estimated from the increase in size of the crystals with storage time.

Differential Scanning Calorimetry Measurements

Glass transition temperature values of the amorphous NFD and NFD–polymer solid dispersions were determined by differential scanning calorimetry (DSC) measurement. Indium was used to calibrate the cell constant and the temperature of the instrument. The DSC cell was purged constantly by dry nitrogen gas flow at 30 mL/min. Crystalline NFD or NFD–polymer mixed powder (approximately 5 mg) in a hermetic aluminum pan was heated to 190°C at a heating rate of 20°C/min, kept at that temperature for 90 s, and then cooled to −80°C at a cooling rate of 40°C/min by pouring liquid nitrogen into a cooling jacket surrounding the DSC cell. The T_g was obtained on the second heating run at a rate of 20°C/min.

The melting point of recrystallized NFD was measured by DSC. After AFM observation, the sample was stored in a desiccator over phosphorous pentoxide at 25°C to complete the recrystallization. Completion of the recrystallization took approximately 3 months for pure NFD, 1 month for NFD–PEG solid dispersions, and a $\frac{1}{2}$ year for NFD–PHPA solid dispersions. The recrystallized sample (5–10 mg) was scratched off from the glass plate into a hermetic aluminum pan, and the melting point of the sample was measured at a heating rate of 20°C/min.

RESULTS AND DISCUSSION

Amorphous NFD Without Polymer

Figure 1 shows typical AFM images of amorphous NFD. Amorphous NFD exhibited a smooth surface immediately after preparation as shown in Figure 1a. The root-mean-square value of the surface roughness was less than 0.5 nm for freshly prepared amorphous samples. After storage at 25°C, structures resembling clusters of curling and branching fibers with a width of approximately 1 μm appeared on the surface as shown in Figure 1b. The size of these structures increased with storage time, suggesting that they were NFD crystals that had formed during storage. The height of the crystals was approximately 1 μm, and hardly this changed even when the scanning area for AFM was covered by NFD crystals. This suggested that NFD crystals preferentially grew along the surface than toward the inner part of the sample. This speculation is supported by the fact that the inner part of the NFD sample after AFM measurements was transparent, indicating that the interior of the samples remained amorphous even after the surface had crystallized. Faster crystal growth of NFD at the surface of amorphous solids has been reported by Zhu et al.[5] They found that the crystal growth of NFD occurred preferentially at the free surface of the amorphous sample when it was exposed to air by removing one glass plate from a sample that had been prepared between two glass plates. The crystal shape reported by Zhu et al.[5] was similar to that shown in Figure 1b.

The crystal form of NFD observed by AFM was determined from the melting point of the recrystallized samples. Figure 2 shows DSC thermograms of crystalline NFD and completely recrystallized NFD, which had been stored as amorphous NFD at 25°C for approximately 3 months after AFM measurements. The recrystallized NFD showed an endothermic peak at approximately 171°C (Fig. 2b), suggesting that a stable form of NFD crystal (Fig. 2a) is formed during storage at 25°C.

Serial AFM images of partially recrystallized amorphous NFD were captured continuously in the same area to determine the crystal growth rate of NFD at

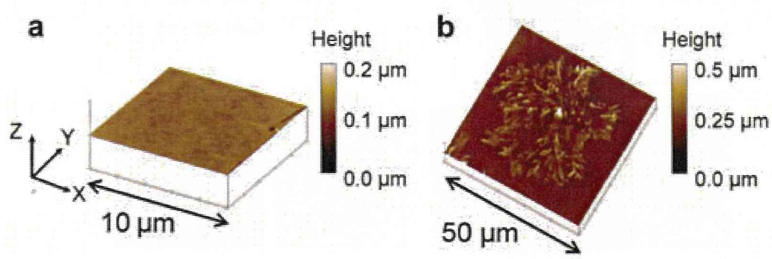

Figure 1. Representative atomic force microscopy images of amorphous nifedipine (a) immediately after preparation and (b) after storage at 25°C.

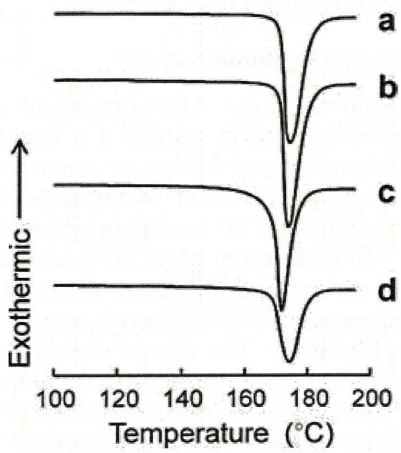

Figure 2. Differential scanning calorimeter thermograms for (a) nifedipine (NFD) in stable form, NFD recrystallized at 25°C from amorphous (b) NFD without polymer, (c) NFD–polyethylene glycol (5%) solid dispersion, and (d) NFD–α,β-poly(N-5-hydroxypentyl)-L-aspartamide (30%) solid dispersion.

the surface. Figure 3 shows typical images representing crystal growth of NFD at the surface. The time required to capture one image was approximately 17 min for this series of measurements. Using image analysis software, the crystal growth rate was determined from the coordinates (x_A, y_A) and (x_B, y_B), which are the end points of one crystal indicated by A in the image after 68 min and B in the image after 102 min, respectively. The growth rate was calculated by dividing the distance between (x_A, y_A) and (x_B, y_B) by the time interval, 34 min. In order to confirm that the physical stimulation from the AFM probe did not affect the crystal growth rate of NFD, AFM images were collected at various time intervals by varying the experimental conditions (scan range, scan speed, and collecting points per line). If the physical stimulus of tapping affected the crystal growth, the estimated growth rates have differed depending on the interval employed for image collection. Growth rates estimated under various experimental conditions are shown in Table 1. Because differences in the estimated growth rates lay within experimental error range regardless of the interval used for image collection, any influence of tapping by the AFM probe on the crystal growth rate was considered to be negligible. The NFD crystal growth rate was also estimated by polarized light microscopy using some pairs of micrographs recorded when the microscope was focused on the surface of the amorphous solid (Table 1). The crystal growth rates of NFD determined from the data obtained by AFM and polarized light microscopy agreed well, and the growth rates determined in the present study were similar to those reported by Zhu et al.[5] for the crystal growth rate at the free surface of amorphous NFD solids.

NFD Solid Dispersions with PEG

The surface of NFD solid dispersions containing PEG was smooth immediately after preparation (images not shown). Figure 4 shows representative AFM images after storage at 25°C for approximately 1 day. NFD–PEG (5%) solid dispersions exhibited dimples at the surface, as shown in Figure 4a. Dimples with a depth of more than 5.7 μm (the operational limit of the AFM probe) were sometimes observed. After longer storage, spiky structures were observed in the dimples, as shown in Figure 4b, and the area with an apparently rough surface increased with time. Crystals were detected by polarized light microscopy in the positions where the dimples, with and without spiky structures, had been observed by AFM. This implies that the formation of dimples and spiky structures is associated with NFD crystallization during storage. Figure 5 shows a partially crystallized NFD–PEG (5%) solid dispersion prepared in a small glass Petri dish. After storage at 25°C for approximately 15 h, some crystals grew at the surface, as circled by dotted lines (Fig. 5a), although most of them were observed randomly in the bulk (Figs. 5a and 5b). These results indicated that NFD crystallization was not always initiated at the surface of NFD–PEG solid dispersions. The dimples at the surface observed by AFM may have been formed by volume reduction upon crystallization of amorphous NFD initiated in the bulk, but not so far from the sample surface. Therefore, it may take some time for the crystals with spiky structures to become apparent at the sample surface, as shown in Figure 4b. These results suggest that AFM measurements discriminate the position where crystallization has initiated (at the surface or in the bulk), and the

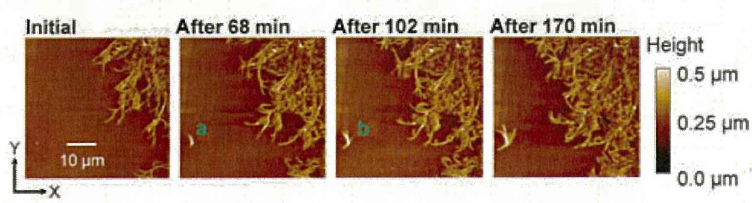

Figure 3. Serial atomic force microscopy images representing crystal growth at the surface of amorphous nifedipine without polymer at ambient temperature (26 ± 1°C).

DOI 10.1002/jps

Table 1. T_g Values Determined by DSC, and NFD Crystal Growth Rates Obtained by AFM and Polarized Light Microscopy at Around 25°C

		AFM Experimental Conditions				Crystal Growth Rate (m/s)	
	T_g (°C)	Scan Range (μm)	Scan Speed (μm/s)	Collected Points Per Line	Collection Interval[a] (min)	AFM	Polarized Light Microscopy
NFD	46.2 ± 0.5[b]	100	75	256	5.3	$(1.2 \pm 0.3) \times 10^{-9}$[c]	$(1.6 \pm 0.4) \times 10^{-9}$[d]
		100	50	256	8.6	$(1.1 \pm 0.3) \times 10^{-9}$[c]	
		50	50	512	8.6	$(1.0 \pm 0.2) \times 10^{-9}$[c]	
		100	50	512	17	$(1.3 \pm 0.4) \times 10^{-9}$[c]	
NFD–PEG (5%)	33.5 ± 0.6[b]	100	150	256	2.6	5.1×10^{-8}	$(7.2 \pm 1.7) \times 10^{-8}$[e]
		80	150	256	2.2	6.3×10^{-8}	
		50	150	256	1.3	4.9×10^{-8}	
		100	100	256	4.3	4.5×10^{-8}	

[a]Time required to collect one image.
[b]Average with standard deviation ($n = 5$).
[c]Average with standard deviation ($n > 9$ points for each five samples).
[d]Average with standard deviation ($n > 5$ points for each five samples).
[e]Average with standard deviation ($n = 6$).
AFM, atomic force microscopy; NFD, nifedipine; PEG, polyethylene glycol.

direction of crystal growth (along the surface or into the bulk): characteristics that are difficult to determine by polarized light microscopy. It should be noted that even though AFM images suggest that crystals grow at the surface of samples, crystallization is not always initiated at the surface.

Although the crystal growth rate of NFD in a solid dispersion with PEG determined by AFM is not the surface growth rate, as described above, the apparent rate was estimated and compared with that obtained by polarized light microscopy. From serial AFM images exemplified by Figure 4b, the crystal growth rate of NFD in solid dispersions containing 5% PEG was determined. Because of possible changes in the NFD crystallization rate by the physical stimulus of tapping, the increase in diameter of the recrystallized domains was measured at various time intervals by varying the experimental scan range (50–100 μm) and scan speed (100–150 μm/s). Figure 6 shows the time profiles of the diameter of the recrystallized domains measured under various experimental conditions: hollow triangles and hollow squares represent the results of measurements using the shortest and the longest time intervals, respectively. The variation in slope appeared to lie within the range of experimental error, and no clear dependence of the growth rate on the time interval for collection was evident. From these results, it is considered that the influence of tapping by the AFM probe on the crystal growth rate is negligible in NFD–PEG solid dispersions. Each growth rate calculated from the slope of the plots shown in Figure 6 is listed in Table 1. The value was of the same order as that obtained by polarized light microscopy at 25°C (Table 1). The crystal growth rate of NFD in the NFD–PEG (5%) solid dispersions was approximately 50 times higher than that in amorphous NFD alone. The T_g value of the NFD–PEG (5%) solid dispersion was approximately 13° lower than that of NFD alone (Table 1), indicating that the matrix mobility of NFD–PEG is higher than that of NFD alone.

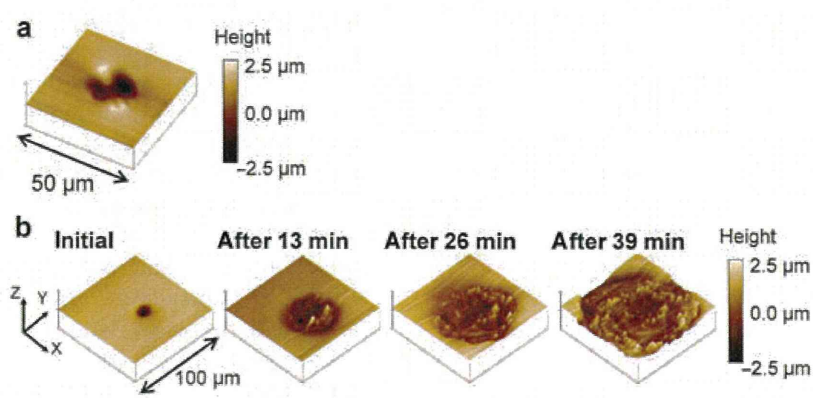

Figure 4. Atomic force microscopy images of nifedipine (NFD)–polyethylene glycol (5%) solid dispersion. (a) Partially recrystallized solid dispersion after storage at 25°C and (b) serial images representing NFD crystal growth at ambient temperature, 26 ± 1°C.

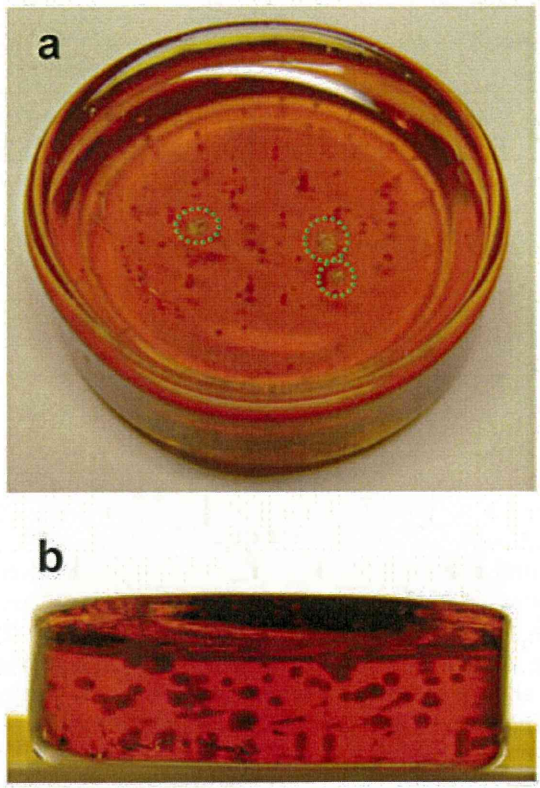

Figure 5. Partially crystallized nifedipine (NFD)–polyethylene glycol (5%) solid dispersion prepared in a small glass Petri dish (inner diameter 23 mm). The sample was stored at 25 C for approximately 15 h. Dotted green circles in the photograph (a) indicate sites of crystallization at the surface. Other dark granular shapes are NFD crystals formed in the amorphous bulk. (a) Photograph taken from top and (b) photograph taken from the side.

The increased molecular mobility of the amorphous matrix may be one of the reasons for the higher crystal growth rate in NFD–PEG solid dispersions. Another possible reason for the higher crystal growth rate may be due to the difference in the crystalline form formed in pure NFD and NFD–PEG solid dispersions during AFM measurements. Although the melting point of the recrystallized NFD in the solid dispersions containing PEG [169°C (Fig. 2c)] suggests that a stable form of NFD crystal is formed during the storage for 1 month, this result may not exclude the possibility that crystals other than stable form have been formed in the solid dispersions during AFM measurements.

NFD Solid Dispersions with PHPA

Figure 7a shows a typical AFM image of partially recrystallized NFD–PHPA solid dispersions stored at 25°C for a few weeks. The diameter and height of the cone-shaped structures increased with storage time.

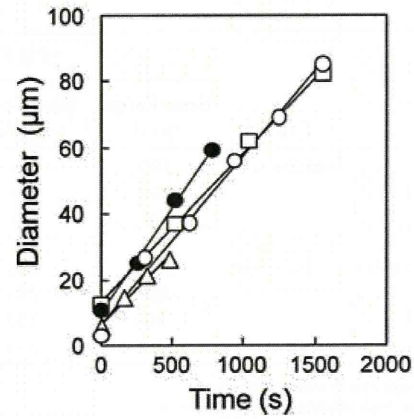

Figure 6. Increase in diameter of crystallized domains at the surface of nifedipine–polyethylene glycol (5%) solid dispersions at ambient temperature, 26 ± 1°C. The time when the first scan had been completed was defined as "time = 0" for each sequential measurement. The measurement conditions for each symbol are as follows (scan range and scan speed): ○ (100 μm, 150 μm/s), ● (80 μm, 150 μm/s), △ (50 μm, 150 μm/s), and □ (100 μm, 100 μm/s).

The melting point of the recrystallized NFD–PHPA (30%) samples stored at 25°C for approximately 6 months (169°C as shown in Fig. 2d) suggests that the crystal with a cone-shaped structure is the stable form of NFD.

Only the cone-shaped structures were observed in the first scan (Fig. 7a), but string-like structures were also observed in the image of the second scan (Fig. 7b). The area covered by the string-like structures increased gradually with each scan, as shown in Figure 7c, which is the image collected after continuous scanning for 34 min. Visual inspection of the area where AFM images were collected revealed loss of transparency in the area, suggesting crystallization of NFD. During the measurements, the size of the originally existing cone-shaped structures did not change (images not shown). Figure 7d shows an image of a different site in the same sample, wherein the AFM probe had not made contact, obtained after scanning the image shown in Figure 7c. No string-like structures were evident. These results suggest that physical stimulation by tapping with the AFM probe caused acceleration of new NFD crystal formation and growth at the surface of solid dispersions containing 30% PHPA. This acceleration effect was also observed for solid dispersions containing up to 70% PHPA. The reason why tapping by the AFM probe only accelerates the formation and growth of string-like crystals is still unclear. NFD is partially immiscible with PHPA. The presence of at least two different phases in the solid dispersion was indicated by the biexponential decay patterns of ^{1}H NMR spin-lattice relaxation.[14]

DOI 10.1002/jps

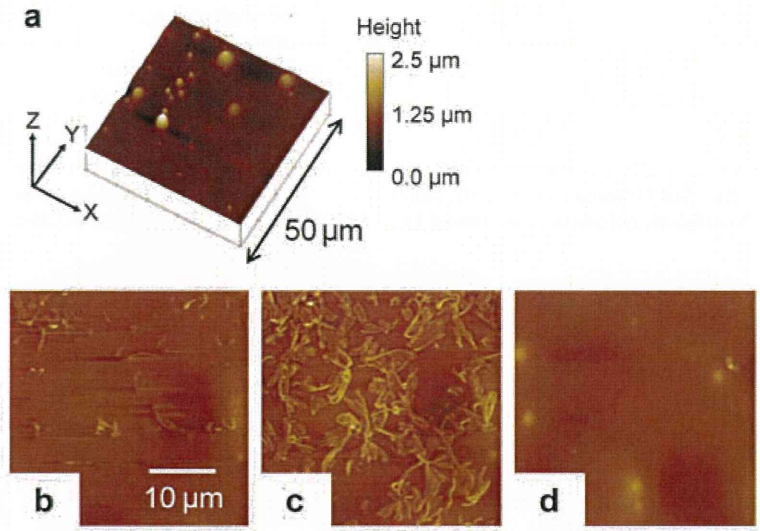

Figure 7. Atomic force microscopy images of nifedipine–α,β-poly(N-5-hydroxypentyl)-L-aspartamide (30%) solid dispersion. (a) The first scan of the partially crystallized sample stored at 25 C for over 1 month, (b) the second scan, (c) after continuous scanning for 34 min, (d) a different site in the same sample after measurement (c). The area for images (b) and (c) corresponds to approximately one-fourth of the bottom-right corner of the image (a).

The finding that the NFD–PHPA solid dispersions exhibit two T_gs has also supported the partial immiscibility between NFD and PHPA.[14] T_gs at 46°C and 70°C for the NFD–PHPA (30%) solid dispersions may correspond to the T_g of amorphous NFD alone and that of the NFD–PHPA matrix, respectively. NFD may be present in a supersaturated state, and may be more sensitive to the physical stimulation of tapping than amorphous NFD without polymer or with PEG.

CONCLUSIONS

Atomic force microscopy was found to be a useful tool for studying the crystallization kinetics of amorphous solids by targeting crystals at the surface. The ability to obtain three-dimensional information at the surface is one of the advantages of AFM, as well as its nanoscale resolution, enabling it to detect minute topographical changes that can indicate the crystal growth rate in a short time. However, two phenomena revealed in this study need to be borne in mind when interpreting the data obtained by AFM measurements: (1) Although crystal structures are captured at the surface of the sample by AFM, the crystal formation may not always be initiated at the surface. The change in surface topography may reflect the growth of crystals from the bulk. (2) Physical stimulation by the AFM probe may affect the crystallization rate, as shown for NFD crystallization in NFD–PHPA solid dispersions.

ACKNOWLEDGMENTS

Part of this work was supported by a grant-in-aid for Research on Publicly Essential Drugs and Medical Devices from The Japan Health Sciences Foundation.

REFERENCES

1. Bunjes H, Rades T. 2005. Thermotropic liquid crystalline drugs. J Pharm Pharmacol 57:807–816.
2. Murdande SB, Pikal MJ, Shanker RM, Bogner RH. 2001. Solubility advantage of amorphous pharmaceuticals: I. A thermodynamic analysis. J Pharm Sci 99:1254–1264.
3. Blagden N, de Matas M, Gavan PT, York P. 2007. Crystal engineering of active pharmaceutical ingredients to improve solubility and dissolution rates. Adv Drug Deliv Rev 59:617–630.
4. Wu T, Yu L. 2006. Surface crystallization of indomethacin below T_g. Pharm Res 23:2350–2355.
5. Zhu L, Wong L, Yu L. 2008. Surface-enhanced crystallization of amorphous nifedipine. Mol Pharm 5:921–926.
6. Liao X, Wiedmann TS. 2006. Formation of cholesterol crystals at a mucin coated substrate. Pharm Res 23:2413–2416.
7. Cassidy AM, Gardner CE, Jones W. 2009. Following the surface response of caffeine cocrystals to controlled humidity storage by atomic force microscopy. Int J Pharm 379:59–66.
8. Price R, Young PM. 2004. Visualization of the crystallization of lactose from the amorphous state. J Pharm Sci 93:155–164.
9. Mahlin D, Berggren J, Alderborn G, Engström S. 2004. Moisture-induced surface crystallization of spray-dried amorphous lactose particles studied by atomic force microscopy. J Pharm Sci 93:29–37.
10. Mahlin D, Berggren J, Gelius U, Engström S, Alderborn G. 2006. The influence of PVP incorporation on moisture-induced surface crystallization of amorphous spray-dried lactose particles. Int J Pharm 321:78–85.
11. Chan KL, Kazarian SG. 2004. FTIR spectroscopic imaging of dissolution of a solid dispersion of nifedipine in poly(ethylene glycol). Mol Pharm 1:331–335.

12. Vippagunta SR, Wang Z, Hornung S, Krill SL. 2007. Factors affecting the formation of eutectic solid dispersions and their dissolution behavior. J Pharm Sci 96:294–304.
13. Bley H, Fussnegger B, Bodmeier R. 2010. Characterization and stability of solid dispersions based on PEG/polymer blends. Int J Pharm 390:165–173.
14. Aso Y, Yoshioka S, Miyazaki T, Kawanishi T, Tanaka K, Kitamura S, Takakura A, Hayashi T, Muranushi N. 2007. Miscibility of nifedipine and hydrophilic polymers as measured by ^{1}H-NMR spin-lattice relaxation. Chem Pharm Bull 55:1227–1231.
15. Rumondor AC, Marsac PJ, Stanford LA, Taylor LS. 2009. Phase behavior of poly(vinylpyrrolidone) containing amorphous solid dispersions in the presence of moisture. Mol Pharm 6:1492–1505.
16. Giammona G, Carlisi B, Plazzo S. 1987. Reaction of α,β-poly(N-hydroxyethyl)-DL-aspartamide with derivatives of carboxylic acids. J Polym Sci Polym Chem Ed 25:2813–2818.

DOI 10.1002/jps

Netsu Sokutei **38** (4) 125-131

解　説

熱分析による非晶質医薬品の結晶化の評価

宮崎 玉樹，阿曽 幸男

（受取日：2011年6月23日，受理日：2011年7月29日）

Evaluation of Crystallization of Amorphous Drugs by Thermal Analysis

Tamaki Miyazaki and Yukio Aso

(Received June 23, 2011; Accepted July 29, 2011)

About half of candidates for active pharmaceutical ingredients are poorly water soluble compounds. Amorphization of poorly water soluble drugs has attracted much attention due to improved dissolution characteristics and bioavailability of amorphous drugs. On the other hand, crystallization during storage is of concern for amorphous drugs. Therefore, evaluation of crystallization of amorphous drug is important for developing stable pharmaceuticals using amorphous drugs. In this article, feasibility of thermal method such as differential scanning calorimeter and isothermal microcalorimeter for evaluating crystallization of amorphous drugs and research topics on the crystallization of amorphous drug are described.
Keywords; amorphous, crystallization, DSC, isothermal microcalorimetry,

1. はじめに

近年の医薬品開発における候補化合物の選択は、標的分子との親和性を指標に行われるため，候補化合物の半数は水に溶けにくいと言われている。このような候補化合物を医薬品として上市するためには，製剤化に際して溶解性を改善するための工夫が必要となる。溶解性の改善のためには可溶性の塩，可溶性のプロドラッグへの変換やシクロデキストリン等との複合体形成など化学的な変換を行うアプローチや，有機溶媒や界面活性剤による可溶化などが考えられる。これらの方法は候補化合物の特性により適用が限られる場合があり，使用可能な有機溶媒や界面活性剤の制限もある。一方，準安定形への結晶化，微粒子化，非晶質化など，候補化合物の物理的状態を変化させることにより溶解性を改善する方法もある。これらの方法は候補化合物を高いエネルギー状態にすることにより溶解性を改善するものであり，適用できる化合物の適用範囲が比較的広く，多くの候補化合物において研究が行われている。しかし，このような物理的なアプローチは，準安定形結晶においては安定形結晶への転移，微粒子化においては凝集や粒子サイズの増大，非晶質化においては結晶化など，安定な状態へ変化する可能性があることが問題点である。このような変化は医薬品の有効性や安全性に影響を及ぼす可能性があるため，医薬品開発においてはこのような変化が起こるかどうか，また，起こるのであればどのようなタイムスケールで起こるのかなどを評価することは非常に重要なことである。我々は物理的なアプローチのなかでも安定状態への変化の可能性が大きいと考えられる非晶質化による溶解性の改善に注目し，ジヒドロピリジン系の医薬品やフェノバルビタールなどをモデルとし，結晶化の速度論的な解析や結晶化に及ぼす温度，湿度，高分子添加剤などの影響について研究を行っている。

本解説においては示差走査熱量測定（DSC）や等温ミクロ熱量測定（IMC）などの熱分析による非晶質医薬品の結晶化の評価の有用性について述べる。

2. DSCによる非晶質薬物の結晶化の評価

非晶質薬物のDSCのデータは非晶質薬物の結晶化を評価するうえで有用な情報を与える。**Fig.1**に非晶質ニフェジピン，ニトレンジピンおよびニルバジピンのDSCの測定例を示す。非晶質固体はある温度においてガラス状態から過冷却液体へ転移し（ガラス転移），それに伴い試料の比熱が変

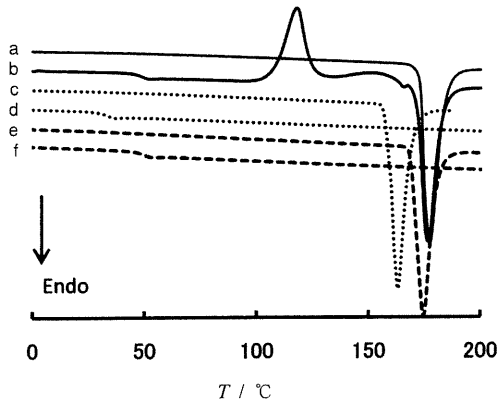

Fig.1 Typical DSC traces for crystalline and amorphous nifedipine (**a**, **b**), nitrendipine (**c**, **d**) and nilvadipine (**e**, **f**).

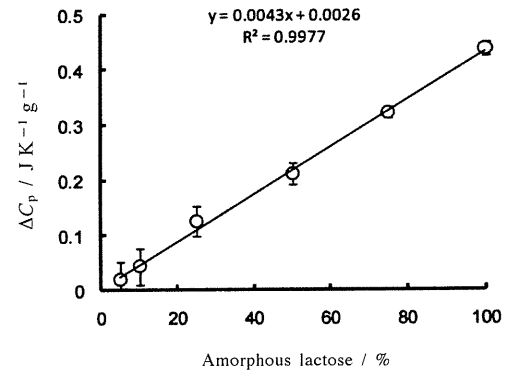

Fig.2 Calibration curve for amorphous lactose in the physical mixture of freeze-dried lactose and lactose hydrate.

化する。**Fig.1(b),(d),(f)**のトレースに示されるように非晶質ニフェジピン，ニルバジピンでは50℃付近に，非晶質ニトレンジピンでは30℃付近にガラス転移に伴うベースラインの断絶が観測された。また，非晶質ニフェジピンにおいては120℃付近にDSCの昇温過程における結晶化にともなう発熱ピークが見られたが，非晶質ニトレンジピンやニルバジピンにおいてはDSCの昇温過程における結晶化に伴う発熱ピークが見られなかった。これらの結果から，ニフェジピンに比べニトレンジピンやニルバジピンは結晶化しにくいと考えることができ，DSCの昇温中における結晶化の有無によって結晶化のしやすさを定性的に評価できる。結晶化のしやすさをより定量的に評価するためには，非晶質薬物の残存量が時間とともにどのように変化するかを明らかにする必要がある。試料中の非晶質薬物の残存量はガラス転移温度（T_g）における比熱の変化量（ΔC_p），結晶化熱（ΔH_c）および融解熱（ΔH_m）を指標に見積もることができる。ただし，ΔH_cを指標として用いる場合にはDSCの昇温過程において，残存する非晶質薬物が定量的に結晶化する必要がある。また，ΔH_mを指標として用いるためにはDSCの昇温過程において結晶化が進行しないことが必要である。非晶質ニフェジピンは**Fig.1(b)**に示すようにDSCの昇温過程において結晶化し，非晶質ニフェジピンの残存量の指標としてΔC_pまたはΔH_cを使用できる。両者の指標を用いることにより同様のタイムコースを得ることができた。ニトレンジピンの調製直後の非晶質試料は**Fig.1(d)**に示すように昇温過程において結晶化しない。しかし，保存後のニトレンジピンの試料においては2つの融解ピークが観測され，2つの融解ピークの比率は試料間でバラツキが見られたため，ΔH_mを指標として用いることはできなかった。そこで，3つの薬物に共通に適用できるΔC_pを用いて，以下の検討を行った。ΔC_pが非晶質薬物の残存量の指標として使用できることを確認するために，**Fig.2**に凍結乾燥によって調製した非晶質乳糖と乳糖水和物の物理混合物についてΔC_pを測定した結果を示す。観測されたΔC_pの値は物理混合物中の非晶質乳糖の比率との間に良好な直線関係が得られた。**Fig.3**に種々の非晶質薬物について測定した非晶質薬物の残存率と保存時間の関係を示す。[1-3] 保存前の試料について得られる$\Delta C_p(0)$とt時間保存した試料の$\Delta C_p(t)$の比から，保存試料中の非晶質薬物の残存率$R(t)$を算出しプロットした。

$$R(t) = \Delta C_p(t) / \Delta C_p(0) \qquad (1)$$

クローズドシンボルは60℃で保存したニフェジピン（T_g＝41℃），ニトレンジピン（T_g＝27℃），ニルバジピン（T_g＝43℃）の結果であり，他のシンボルは45℃で保存したニフェジピン，フェノバルビタール（T_g＝37℃），フロプロピオン（T_g＝55℃)およびアセトアミノフェン（T_g＝25℃)の結果を示す。また，図に示す曲線はAvrami式(式(2))にフィットして得られたものである。

$$R(t) = \exp\{-kt^n\} \qquad (2)$$

ここで，nは結晶化のメカニズムに依存する定数であり，薬物によって異なる。**Fig.3**の非晶質薬物の残存率のタイムコースから示されるように結晶化のしやすさは薬物によって大きく異なった。T_gが高い薬物ほど結晶化しにくい傾向が見られるが，例外も見られる。例えば，ニフェジピン（T_g＝41℃）とニルバジピン（T_g＝43℃）を比較すると，ほぼ同様のT_gにもかかわらず，ニルバジピンの結晶化は非常に遅かった。また，ニルバジピンにくらべフロプロピオン（T_g＝55℃）のT_gは高いが，45℃で保存したフロプロピオ

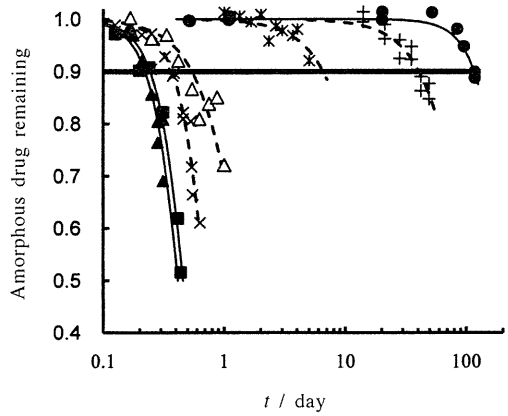

Fig.3 Typical time courses for crystallization of amorphous drugs stored at 60 (closed symbol) or 45 ℃.
▲, nifedipine, 60 ℃; ■, nitrendipine, 60 ℃; ●, nilvadipine, 60 ℃; △, nifedipine, 45 ℃; ＊, phenobarbital, 45 ℃; +, flopropine, 45 ℃; ×, acetaminophen, 45 ℃.

ンは，60 ℃で保存したニルバジピンより速やかに結晶化が進行した。T_gは非晶質薬物の結晶化のしやすさの指標になるが，T_g以外の因子も結晶化のしやすさに関与していることを示唆する結果と考えられる。従って，結晶化速度に影響を及ぼす因子を明らかにすることは，非常に興味深いことと考える。

以下の議論においては非晶質薬物の残存率が0.9になる時間t_{90}を結晶化のしやすさの指標として用いる。結晶化のしやすさに影響を及ぼす因子を考察するために，類似のジヒドロピリジン環構造を有するニフェジピン，ニトレンジピン，ニルバジピンについて，t_{90}に及ぼす温度，湿度の影響を検討し，その結果を**Fig.4**に示す。オープンシンボルは乾燥状態の試料について得られた結果である。ニルバジピンとニトレンジピンは温度が低いほどt_{90}が長くなり，結晶化が起こりにくくなる。それに対し，ニフェジピン（□）のt_{90}の温度依存性はT_g（$1000/T=3.1$）付近で断絶が見られた。Ishidaらによってもニフェジピンの結晶成長速度の温度依存性にT_g付近で断絶があることが報告されている。Ishidaらは検討した温度範囲において生成する結晶形が同じであることから，結晶成長速度の温度依存性のT_g付近における断絶は結晶化メカニズムがT_g付近で変化すると考えており，T_g以上の温度においては拡散が律速（diffusion controlled）のメカニズムにより結晶化するのに対し，T_g以下の温度ではNon-diffusion controlledメカニズムによって起こると考えている。[4]

Fig.4のクローズドシンボルは非晶質ニルバジピンを一定

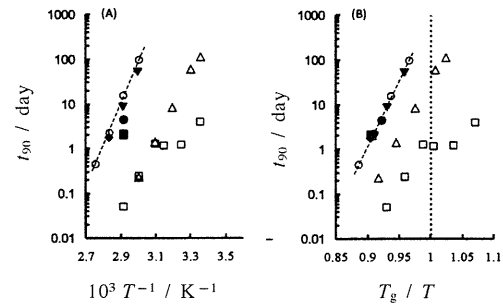

Fig.4 Temperature dependence of t_{90} for amorphous nifedipine (□), nitrendipine (△) and nilvadipine (○, ◆, ■, ●, ▼).
Relative humidity: □, △, ○, 0%; ◆, 11%; ▼, 23%; ●, 56%; ◆, 75%.

の相対湿度に保存し，吸湿させた試料について得られた結果を示す。保存湿度が高く，吸湿量が多いと考えられる試料ほどt_{90}が短かった。また，吸湿させた試料のT_gは保存湿度が高い試料ほど低かった。結晶化は核生成と結晶成長の2つの過程によって進行し，これらの過程の速度の温度依存性は分子運動性の因子（＝粘度）と熱力学的な因子（＝結晶と非晶質の自由エネルギーの差に起因する因子と結晶化によって新たな界面が生成することによる自由エネルギーの増えに起因する因子）によって支配されると報告されている。[5] **Fig.4(B)**に示すように，吸湿によるT_gの低下を考慮し，t_{90}の値をT_g/Tに対してプロットすると，ニルバジピンのt_{90}のデータは1つの直線上に集まった。T_gの変化は試料の粘度（＝分子運動性）の変化を反映することから，試料の吸湿は主に分子運動性を変化させ，結晶化のしやすさに影響していると考えられる。吸湿による分子運動性の変化が結晶のしやすさに影響することはニトレンジピンやニフェジピンにおいても観察されている。[3] しかし，高分子が共存する場合には水は分子運動性に影響を及ぼす他に，高分子とともに溶媒として作用し，過飽和度に影響することが報告されている。[6] 水の結晶化に及ぼす影響についてさらに検討する必要があると考えられる。

ニフェジピン，ニトレンジピン，ニルバジピンはジヒドロピリジン環を有し，類似の化学構造をもつが，ニルバジピンのt_{90}の値は他の2つの薬物のt_{90}の値と大きく異なった。分子運動性の因子（＝T_g）の影響を除くためにT_g/Tに対してプロットしても薬物間のt_{90}の違いは見られ，熱力学的因子が薬物間のt_{90}の差をもたらしているものと考えられる。結晶と非晶質の自由エネルギーの差（ΔG_v）はHoffman式（式(3)）によって見積もることができる。[7]

$$\Delta G_v = \{\Delta H_m \times (T_m - T) \times T\}/T_m^2 \qquad (3)$$

Table 1 Thermodynamic parameters of amorphous drugs.

Drug	ΔG_v at T_g J m^{-3}	T_g / ℃	T_m / ℃	ΔH_m / kJ mol^{-1}
Nifedipine	3.13 ×10^7	41.3 ±0.2	172.5 ±0.5	37.9 ±0.8
Nitrendipine	3.07 ×10^7	27.1 ±0.4	156.0 ±0.6	39.0 ±0.5
Nilvadipine	2.77 ×10^7	42.8. ±0.4	168.1 ±0.4	39.1 ±0.7

ここで，ΔH_m，T_mは融解熱と融点を表す。

Table 1に示すように，T_gにおける単位体積当たりのΔG_vの値はニフェジピン>ニトレンジピン>ニルバジピンの順である。従って，**Fig.4(B)**に示すT_gにおける結晶化のしやすさの順と同じであり，結晶と非晶質の自由エネルギーの差が非晶質医薬品の安定性の差に一部寄与していると考えられる。しかし，ΔG_vの違いのみで安定性の差を説明するためにはその差が小さく，界面自由エネルギーの寄与や結晶化メカニズムの違いも関与していると考えられる。

ポリビニルピロリドン（PVP）やヒドロキシプロピルメチルセルロース（HPMC）などの水溶性高分子添加剤は非晶質薬物の結晶化を抑制することが知られている。結晶化の抑制は，薬物に比べ高いT_gを有する高分子添加剤を添加することにより，薬物単独に比べT_gが上昇し，分子運動性が抑制されるためであると言われている。また，T_gの変化の見られないような少量の高分子の添加によっても結晶化が抑制されることから，薬物と高分子の相互作用も結晶化抑制に寄与していると考えられる。薬物－高分子相互作用の結晶化速度に及ぼす影響を検討するために，分子運動性に差がないと考えられるニトレンジピンエナンチオマーを用い，セルロース誘導体を添加した固体分散体中の結晶化速度を明らかにした。[8] ニトレンジピンは不斉炭素を有し，光学活性カラム（CHIRALCEL OJ-H，ダイセル化学工業(株)）を用いたHPLCにより光学分割を行うことができる。230 nmの紫外光に対する円偏光二色性の符号に基づきHPLCにおいて先に溶出するエナンチオマーを(-)-ニトレンジピン，後から溶出するものを(+)-ニトレンジピンと記す。得られたそれぞれのエナンチオマーのT_g，T_mなどの物理化学特性は同一であった。**Fig.5**に結晶化のタイムコースを示す。薬物単独の場合はエナンチオマー間で結晶化のタイムコースに差は見られなかった。また，不斉炭素を有するがランダムな立体配置をとっているため光学活性を有しないPVPを添加した場合もエナンチオマー間で結晶化のタイムコースに差は見られなかった。それに対し，セルロース由来であり，光学活性を有するHPMCを添加した固体分散体においては(+)-ニトレンジピンは(-)-ニトレンジピンに比べ結晶化が遅いことが示された。このエナンチオマー間の安定性の差は相互作用の差によるものと考えられる。ニトレンジピンの結晶化のt_{90}値を**Table 2**に示す。50 ℃や60 ℃においては，HPMCを添加した(+)-ニトレンジピンは(-)-ニトレンジピンに比べ1.5倍程度t_{90}が長く，HPMCは(+)-ニトレンジピンをより安定化するが，40 ℃においては，エナンチオマー間でt_{90}に差が見られなかった。その理由を十分に説明することはできないが，以下のような説明が可能かもしれない。結晶化速度の温度依存性は，先に述べたように分子運動性の因子と熱力学的な因子によって支配されるが，T_g付近やそれより低い温度領域では分子運動性の因子が支配的であると言われている。HPMCを添加したニト

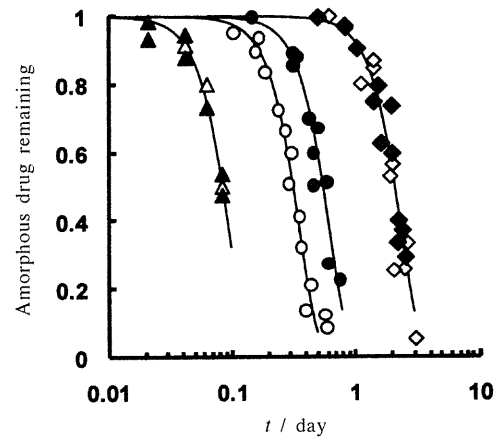

Fig.5 Time courses of crystallization of (+)-nitrenndipine (closed symbols) and (-)-nitrendipine (open symbols) in the absence (△, ▲) and presence of 10%PVP (◇, ◆) or 10%HPMC(○, ●) at 60 ℃.

Table 2 t_{90} for crystallization of nitrendipine enantiomers.

T / ℃	Polymer	t_{90} / h (-)-nitrendipine	(+)-nitrendipine
40	None	41	41
	10% HPMC	235	230
50	None	5.7	5.7
	10% PVP	250	250
	10% HPMC	17	25
60	None	1.1	1.1
	10% PVP	25	25
	10% HPMC	3.9	6.8

Table 3 Cohesive energy density of nitrendipine enantiomers at 25 ℃.

polymer	Cohesive energy density / $\times 10^8$ J m^{-3}	
	(S)-nitrendipine	(R)-nitrendipine
None	5.36	5.37
PVP	5.00	4.93
HPMC	5.56	5.58

レンジピンのT_gはエナンチオマー間で差がなく（(+)-ニトレンジピン-10 % HPMC: 33.0 ± 0.7 ℃，(-)-ニトレンジピン-10 % HPMC: 33.1 ± 1.0 ℃），分子運動性にエナンチオマー間で差がない。従って，40 ℃においてはエナンチオマー間でt_{90}に差が見られなかったものと考えられる。

薬物-高分子相互作用の検出は赤外吸収スペクトルによって行われることが多いが，HPMCを添加したニトレンジピンの赤外吸収スペクトルはエナンチオマー間で大きな差が見られなかった。そこで，分子動力学的シミュレーションによる凝集エネルギーを指標として，相互作用の差を検出できるか検討した。凝集エネルギーは，セル中に存在する原子1つ1つをそれぞれ無限大の距離に引き離すために必要なエネルギーを表わし，高分子間の相互作用の大きさにエナンチオマー間で差があれば凝集エネルギーに反映されるとの仮定に基づいている。ニトレンジピンエナンチオマーとPVPまたはHPMCの混合物のモデルをMaterials Studioソフトウェア（Accelrys）のAmorphousCellモジュールを用いて作成した。混合物のモデルはニトレンジピンエナンチオマー20分子とモノマーユニット数が10の高分子3分子を用いた(薬物と高分子の重量比　約1:1)。Discoverモジュールを用いて分子動力学シュミュレーションを行い，凝集エネルギーを算出した。力場はpcffを用いた。25 ℃でエネルギー極小化処理を行った後，圧力一定条件下で5,000ステップの平衡化を行った。次に，平衡化されたセルについて体積一定条件下で100,000 ~ 2,000,000ステップの動力学計算を行い，原子の座標の軌跡を数フレーム得た。得られたフレームについて凝集エネルギーを算出した。**Table 3**に示すように凝集エネルギーはエナンチオマー間で差は見られなかった。t_{90}のエナンチオマー間の差は1.5倍程度であり，HPMCとニトレンジピンエナンチオマー間の相互作用の差は赤外吸収スペクトルや凝集エネルギーには反映されないような小さな差であると考えられる。

3. IMCによる非晶質薬物の結晶化の評価

IMCは，DSCに比べ高い精度で温度制御が可能であり（$\pm 10^{-6}$ K），ノイズが少なく，安定なベースラインが得られるため，DSCに比べ高感度な測定が可能である。従って，

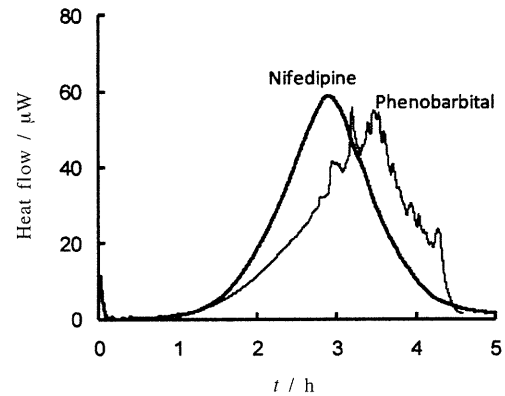

Fig.6 Typical heat flow-time curves of amorphous nifedipine and phenobaribital at 65 ℃.

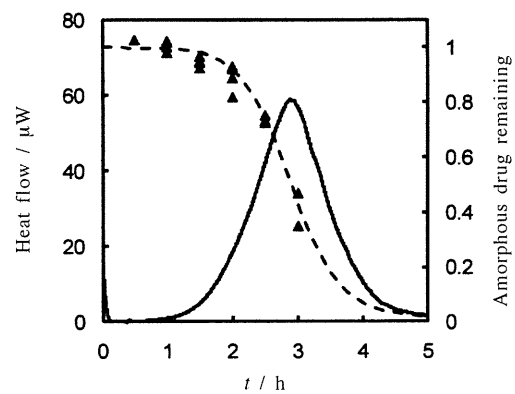

Fig.7 Comparison of amorphous nifedipine remaining estimated from IMC (---) and DSC (▲).

結晶化の進行が緩やかな温度条件においても，結晶化に伴う発熱を経時的に測定することが可能であり，非晶質医薬品の結晶化の過程を直接的に観測できる。[9] **Fig.6**に非晶質ニフェジピン，フェノバルビタールの測定例を示す。いずれの薬物も3から4時間後に発熱のピークが観測された。Heat flowが0に戻った試料についてDSCの測定を行うと結晶ニフェジピンあるいは結晶フェノバルビタールの融解による吸熱ピークが観測された。このことから，**Fig.6**に示されるHeat flowは非晶質ニフェジピンあるいはフェノバルビタールの結晶化に基づく発熱であることが分かる。全体のHeat flow curveを積分して得られる熱量（H）と時間tまでのHeat flowの積分値（H_t）との比（H_t/H）は結晶化の進行度x_tを表し，$1-x_t$を計算することにより試料に残存する非晶質薬物の残存率が得られる。IMCのHeat flow

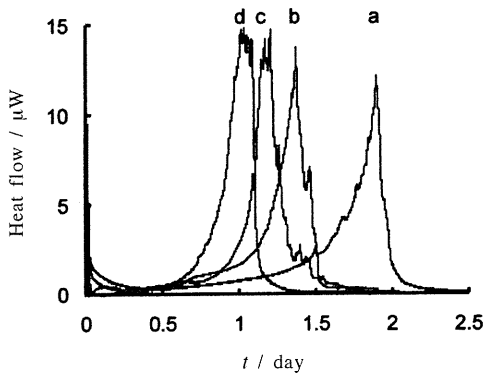

Fig.8 Effect of relative humidity in the ample on heat flow-time curve of amorphous nifedipine at 50 ℃.
Relative humidity: b, 22%; c, 40%; d, 56%.
a: ample was purged by dry nitrogen before the ample was closed.

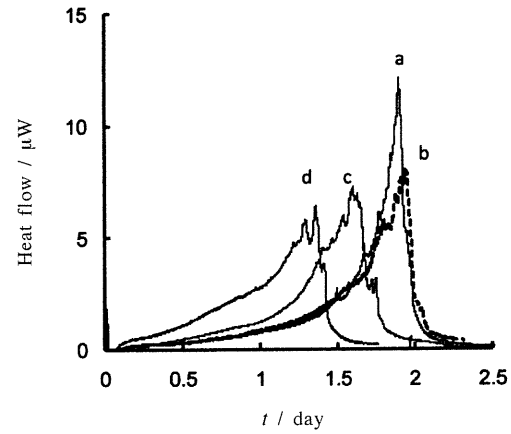

Fig.9 Effect of thermal history on heat flow-time curve of amorphous nifedipine at 50℃.
a, initial; b, -20℃ for 17 months; c, 5℃ for 40 days; d, 25℃ for 2days.

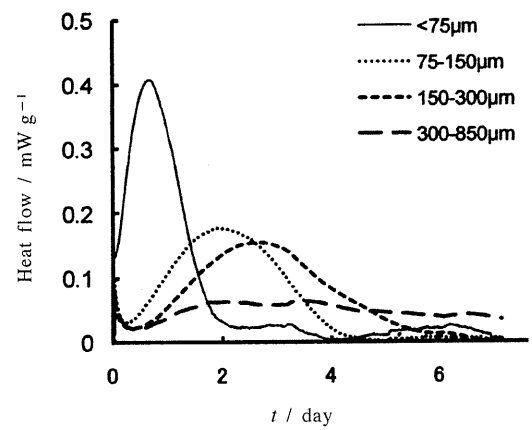

Fig.10 Effect of particle size on heat flow-time curve of amorphous nifedipine at 25℃.

から算出した残存率を**Fig.7**に示す。破線で示されるIMCから得られた非晶質薬物の残存率は，別途，T_gにおける比熱の変化量をもとに算出した残存率（▲)のタイムコースとほぼ一致した。

IMCでは1つの試料で結晶化のタイムコースが得られるため，さまざまな因子が結晶化速度に及ぼす影響を比較的簡便に明らかにできる。例えば，測定前に種々の湿度に1時間保存したアンプルに非晶質ニフェジピンを入れ，そのHeat flowを測定すると，**Fig.8**に示すように，保存湿度が高いほど発熱のピーク到達時間が短く，結晶化が速やかに進行していることが分かる。これは，アンプル内の水分がニフェジピンのT_gを低下させ，その結果，分子運動性が高まり，結晶化が促進されたものと考えられる。このように，結晶化速度に及ぼす水分の影響を比較的簡便に評価することができる。また，結晶化速度に及ぼす熱履歴の影響もIMCのHeat flowのタイムコースから明らかにできる。**Fig.9**に種々の温度条件で保存した非晶質ニフェジピンのHeat flowの測定例を示す。5℃で40日あるいは25℃で2日保存した試料では，発熱のピーク到達時間が調製直後の試料に比べ短かった。これは，IMC測定前の保存の間に結晶核の生成などの非晶質マトリックスの変化が起こり，結晶化に伴う発熱が観測されるまでのラグタイムが短くなった結果と考えられる。−20℃で17か月保存したサンプルは調製直後の試料と同様のタイムコースが得られ，非晶質マトリックスの変化は起こらなかったものと考えられる。

最近，非晶質固体の表面における結晶成長は非晶質固体の内部における結晶成長比べ1オーダー以上速やかに進行することが報告されている。[10,11] 非晶質医薬品の表面の結晶化は溶解性へ影響を及ぼすと予想され，非晶質固体の表面と内部の安定性の違いを評価し，溶解性の改善に対する表面の結晶化のインパクトを理解することは安定な非晶質医薬品を開発する上で非常に重要である。IMCはこのような非晶質固体の表面と内部の安定性の違いの評価に有用であると考えられる。**Fig.10**は粒子サイズを変えて表面と内部の比率を変化させた非晶質ニフェジピンのHeat flow曲線を示す。試料の粉砕，ふるい分け，試料のIMC用のアンプルへの封入は乾燥窒素中で行い，4つの試料は同時に測定したものである。粒子サイズの小さな試料ほど短時間で発熱が観測された。IMC測定後にDSCの測定を行った結果，

300～850 μmの粒子径の試料はガラス転移が観測され，非晶質ニフェジピンが残存することが示されたが，75 μm以下の粒子径の試料についてガラス転移は観測されず，結晶ニフェジピンの融解のみが観測された。試料の表面積とIMC測定によって得られる結晶化速度に関する情報を詳細に解析することにより，非晶質試料の表面と内部の安定性を定量的に比較できるものと考える。

4. おわりに

DSCやIMCなどの熱分析は，非晶質薬物の結晶化のしやすさを評価し，非晶質医薬品の安定性に影響を及ぼす因子を明らかにする上で有用な手法である。これらの手法を活用することにより，安定な非晶質医薬品の開発が促進されることを期待する。

文　献

1) Y. Aso, S. Yoshioka, and S. Kojima, *J. Pharm. Sci.* **89**, 408 (2000).
2) T. Miyazaki, S. Yoshioka, Y. Aso, and S. Kojima, *J. Pharm. Sci.* **93**, 2710 (2004).
3) T. Miyazaki, S. Yoshioka, Y. Aso, and T. Kawanishi, *Int. J. Pharm.* **336**, 191 (2007).
4) H. Ishida, T. Wu, and L.Yu, *J. Pharm. Sci.* **96**, 1131 (2007).
5) V. Andronis and G. Zografi, *J. Non-crystalline solid* **271**, 236 (2000).
6) P. J. Marsac, H. Konno, A. C. F. Rumondor, and L. S. Taylor, *Pharm. Res.* **25**, 647 (2008).
7) J. D. Hoffman, *J. Chem. Phys.* **29**, 1192 (1958).
8) T. Miyazaki, Y. Aso, S. Yoshioka, and T. Kawanishi, *Int. J. Pharm.* **407**, 111 (2011).
9) Y. Aso, S. Yoshioka, and S. Kojima, *Thermochimica Acta* **380**, 199 (2001).
10) T. Wu and L. Yu, *Pharm. Res.* **23**, 2350 (2006).
11) L. Zhu, L. Wong, and L. Yu, *Molecular Pharm.* **5**, 921 (2008).

要　旨

医薬品候補化合物は半数が水に溶けにくいと言われている。水に溶けにくい医薬品の溶解性を改善する方法として，非晶質化が注目されている。非晶質化した医薬品は保存中に，より安定な結晶状態に変化する可能性があり，非晶質医薬品の結晶化を評価することは医薬品開発において重要である。本解説においては熱分析（DSC，IMC）を用いて非晶質医薬品の結晶化を評価した例を紹介し，これらの手法の有用性について述べる。また，非晶質医薬品の結晶化評価における最近のトピックを紹介する。

宮崎玉樹　Tamaki Miyazaki
国立医薬品食品衛生研究所，National Institute of Health Sciences, TEL.03-3700-8547, FAX. 03-3707-6950
E-mail: miyazaki@nihs.go.jp
研究テーマ：医薬品の安定性評価
趣味：旅行

阿曽幸男　Yukio Aso
国立医薬品食品衛生研究所，National Institute of Health Sciences, TEL.03-3700-8547, FAX. 03-3707-6950
E-mail: aso@nihs.go.jp
研究テーマ：医薬品の物性評価と安定性
趣味：音楽鑑賞

International Journal of Pharmaceutics 407 (2011) 111–118

Contents lists available at ScienceDirect

International Journal of Pharmaceutics

journal homepage: www.elsevier.com/locate/ijpharm

Differences in crystallization rate of nitrendipine enantiomers in amorphous solid dispersions with HPMC and HPMCP

Tamaki Miyazaki [a,*], Yukio Aso [a], Sumie Yoshioka [b], Toru Kawanishi [a]

[a] Division of Drugs, National Institute of Health Sciences, 1-18-1 Kamiyoga, Setagaya-ku, Tokyo 158-8501, Japan
[b] School of Pharmacy, University of Connecticut, Storrs, CT, United States

ARTICLE INFO

Article history:
Received 21 October 2010
Received in revised form
21 December 2010
Accepted 19 January 2011
Available online 26 January 2011

Keywords:
Nitrendipine
Enantiomer
Chiral polymer
Solid dispersions
Crystallization

ABSTRACT

To clarify the contribution of drug–polymer interaction to the physical stability of amorphous solid dispersions, we studied the crystallization rates of nitrendipine (NTR) enantiomers with identical physicochemical properties in the presence of hydroxypropylmethylcellulose (HPMC), hydroxypropylmethylcellulose phthalate (HPMCP) and polyvinylpyrrolidone (PVP). The overall crystallization rate at 60 °C and the nucleation rate at 50–70 °C of (+)-NTR were lower than those of (−)-NTR in the presence of 10–20% HPMC or HPMCP. In contrast, similar crystallization profiles were observed for the NTR enantiomers in solid dispersions containing PVP. The similar glass transition temperatures for solid dispersions of (−)-NTR and (+)-NTR suggested that the molecular mobility of the amorphous matrix did not differ between the enantiomers. These results indicate that the interaction between the NTR enantiomers and HPMC or HPMCP is stereoselective, and that differences in the stereoselective interaction create differences in physical stability between (−)-NTR and (+)-NTR at 50–70 °C. However, no difference in physical stability between the enantiomers was obvious at 40 °C. Loss of the difference in physical stability between the NTR enantiomers suggests that the stereoselective interaction between NTR and the polymers may not contribute significantly to the physical stabilization of amorphous NTR at 40 °C.

1. Introduction

Nifedipine analogues are used for treatment of cardiovascular disorders. Most of them are poorly water soluble and their bioavailability is low when administered orally in crystal form. To improve the bioavailability by increasing the dissolution rate and solubility, amorphous solid dispersions of nifedipine analogues have been studied over the past few decades (Suzuki and Sunada, 1998; Chutimaworapan et al., 2000; Vippagunta et al., 2002; Hirasawa et al., 2003a,b, 2004; Tanno et al., 2004; Karavas et al., 2005, 2006; Wang et al., 2005, 2007; Kim et al., 2006; Konno and Taylor, 2006; Huang et al., 2008; Marsac et al., 2008; Rumondor et al., 2009a,b). Drugs in an amorphous state are more easily dissolved in water than their crystalline counterparts. However, recrystallization to a thermodynamically stable form during long-term storage is a matter of concern. The physical stability of amorphous solid dispersions (crystallization tendency) has been reported to correlate with several factors, such as molecular mobility (Aso et al., 2004; Miyazaki et al., 2007), drug–excipient interactions and miscibility (Matsumoto and Zografi, 1999; Marsac et al., 2006, 2009; Miyazaki et al., 2004, 2006, 2007; Konno and Taylor, 2006; Haddadin et al., 2009; Tao et al., 2009; Telang et al., 2009). The crystallization rate of amorphous nitrendipine (NTR) increases with a decrease in the glass transition temperature (T_g) associated with water sorption, indicating that molecular mobility, in terms of T_g, is correlated with physical stability. However, amorphous nilvadipine is more stable than nifedipine, even though the two had similar T_g values, indicating that the difference in physical stability between nilvadipine and nifedipine might be attributable to differences in chemical structure (Miyazaki et al., 2007). Hydrogen bond interaction between felodipine and hydroxypropylmethylcellulose (HPMC) or hydroxypropylmethylcellulose acetate succinate is considered to decrease the nucleation rate of felodipine, since no significant change in molecular mobility, reflected in T_g value, has been observed (Konno and Taylor, 2006). Also, drug–excipient miscibility is reportedly related to the physical stability of nifedipines. Drug crystallization has been observed to occur earlier in solid dispersions showing phase separation due to low miscibility of the drug with the excipient polymers (Rumondor et al., 2009a,b; Marsac et al., 2010). In order to develop stable amorphous solid dispersions, it is important to clarify the relative significance of these factors for the physical stability of amorphous solid dispersions. Therefore, designing a model system that is as simple as possible is the key to evaluation of each individual factor.

NTR has an asymmetric carbon (Fig. 1), and is available as a mixture of both enantiomers. These enantiomers can be resolved by chiral chromatography. Since both enantiomers have identical physical and chemical properties, including molecular mass, T_g,

* Corresponding author. Tel.: +81 3 3700 1141; fax: +81 3 3707 6950.
E-mail address: miyazaki@nihs.go.jp (T. Miyazaki).

0378-5173/$ – see front matter © 2011 Elsevier B.V. All rights reserved.
doi:10.1016/j.ijpharm.2011.01.035

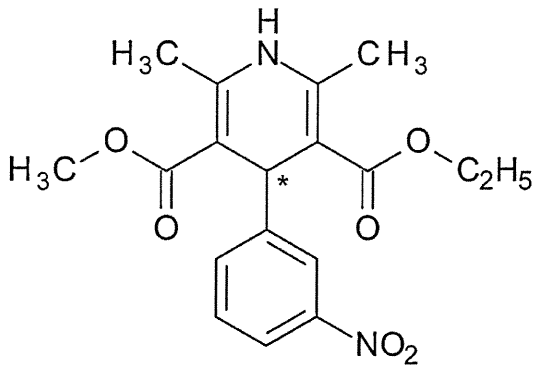

Fig. 1. Chemical structure of NTR. The asterisk represents asymmetric carbon.

melting point and density, the effects of molecular mobility and chemical structure on their physical stability are expected to be the same. Therefore, solid dispersions of NTR enantiomers may provide a useful model system for studies of drug–polymer stereoselective interaction. In the present study, HPMC and hydroxypropylmethylcellulose phthalate (HPMCP) were used as chiral polymers, and polyvinylpyrrolidone (PVP), an achiral polymer, was selected as a control to investigate the effect of drug–polymer interaction on the physical stability of amorphous NTR enantiomers. The overall crystallization rates were determined from the time-profiles of amorphous drug remaining, as measured by differential scanning calorimetry (DSC). Furthermore, the nucleation and the crystal growth rates of each NTR enantiomer in the solid dispersions containing HPMC, HPMCP or PVP were determined by polarized light microscopy. Measurements of T_g and Fourier-transform infrared spectra (FT-IR) were carried out for evaluation of molecular mobility and drug–polymer interactions, respectively.

2. Materials and methods

2.1. Materials

PVP (PVP10) and HPMC (USP grade) were purchased from Sigma–Aldrich, Inc. HPMCP (HP-55) was kindly obtained from Shin-Etsu Chemical Co., Ltd.

NTR (Wako Pure Chemical Industries Ltd.) was resolved on a CHIRALCEL OJ-H column (Daicel Chemical Industries, Ltd., 10 mm × 250 mm) into two fractions of each enantiomer with a mobile phase of n-hexane/ethanol (100/15, flow rate: 4 ml/min). A 500 μl of 1% NTR solution in n-hexane/ethanol (1/1) was injected, and ultraviolet spectrophotometric detection was carried out at 254 nm. The circular dichroism spectrum of the first fraction exhibited a negative peak at around 360 nm, and the second one exhibited a positive peak. Therefore, the first and second fractions of NTR were designated (−)-NTR and (+)-NTR, respectively. The optical purity of each enantiomer was determined to be more than 99.96%, and the amount of photo degradation product of NTR was determined to be less than 0.03% by liquid chromatography, on a CHIRALCEL OJ-H column (Daicel Chemical Industries, Ltd.,

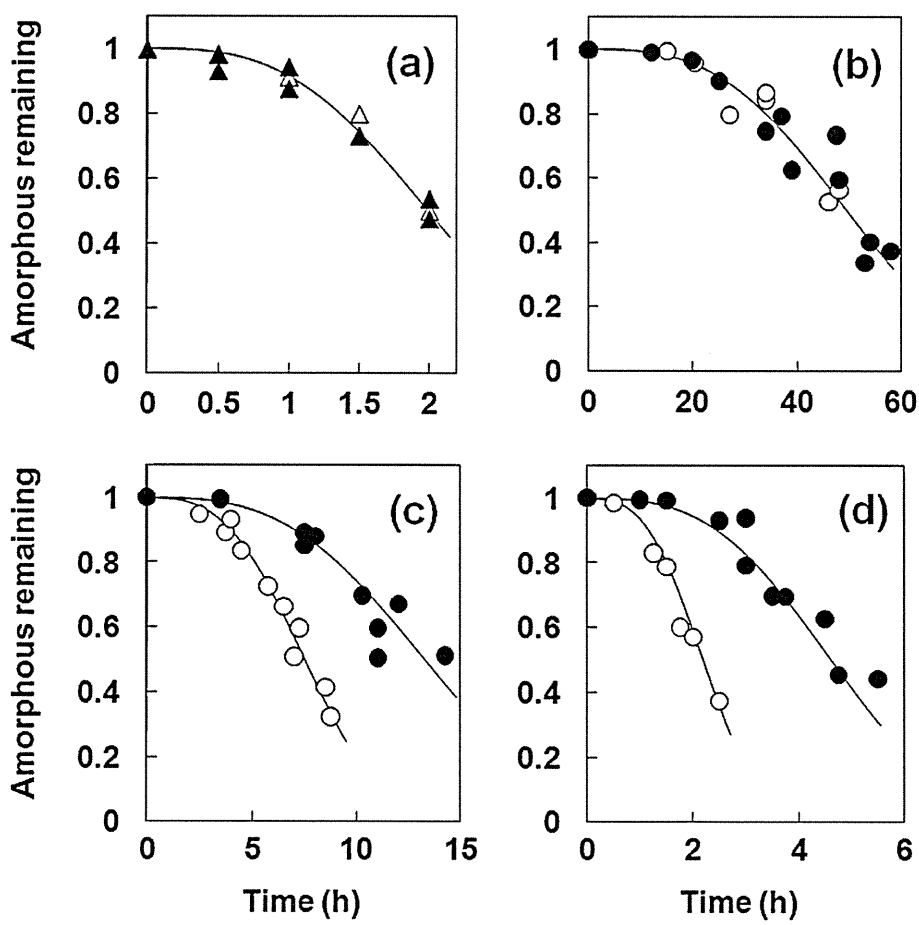

Fig. 2. Crystallization profiles of each NTR enantiomer alone ((a); △, ▲) and the enantiomers in solid dispersions (○, ●) with (b) 10% PVP, (c) 10% HPMC and (d) 10% HPMCP at 60 °C. Open symbols represent (−)-NTR and solid symbols represent (+)-NTR. The lines in the figures represent the best fit of the Avrami equation.

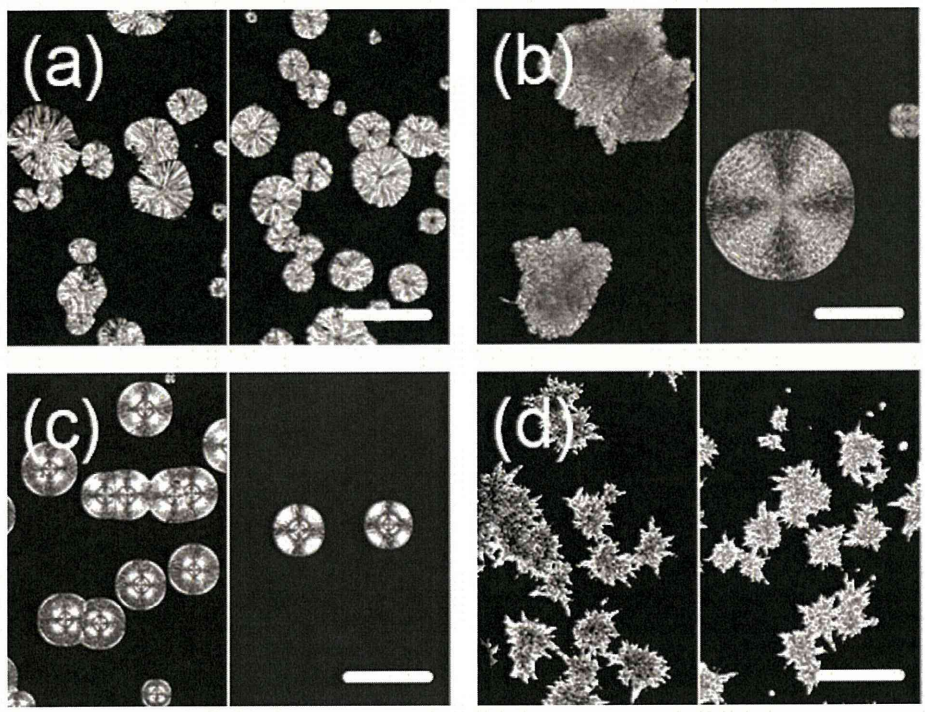

Fig. 3. Typical crystal shape observed for the amorphous NTR enantiomers and their solid dispersions: (a) without polymer, (b) 10% HPMC, (c) 10% HPMCP and (d) 10% PVP. The left side of each micrograph was taken from the (−)-NTR samples, and the right side from the (+)-NTR samples. The bars in the micrographs correspond to 100 μm.

4.6 mm × 250 mm) with a mobile phase of n-hexane/ethanol = 10/1 (1 ml/min). Since NTR is a photo sensitive compound, NTR samples were handled under dim light (<120 lx).

2.2. Determination of the overall crystallization rate of amorphous NTR enantiomers

Amorphous solid dispersions of the NTR enantiomers were prepared by melt-quenching drug–polymer mixtures. One NTR enantiomer and a polymer were initially dissolved in a solvent that was suitable for both components. Ethanol/acetone (1:1) was used for the NTR–HPMC and NTR–HPMCP combinations, and ethanol was used for the NTR–PVP combination. Next, the solvent was rotary-evaporated to obtain a homogeneous drug–polymer mixture. Approximately 4 mg of the pulverized mixture was weighed into an aluminum pan for DSC, and was kept at around 180 °C in the cell of a DSC (DSC2920, TA Instruments) for approximately 2 min under dry nitrogen gas flow (30 ml/min). The melted sample was transferred to a desiccator containing phosphorus pentoxide, and the desiccator was stored at a constant temperature of 30–70 °C. For the pure NTR enantiomer, the resolved enantiomer crystal (4 mg) was melt-quenched as described above to obtain an amorphous sample.

After certain periods of time, the change in heat capacity (ΔC_p) at T_g was measured for the stored amorphous samples by DSC at a heating rate of 20 °C/min. The amount of amorphous drug remaining in the sample at time t, $x(t)$, was calculated according to Eq. (1):

$$x(t) = \frac{\Delta C_{pt}}{\Delta C_{p0}} \tag{1}$$

where ΔC_{pt} and ΔC_{p0} are the ΔC_p values at time t and initially, respectively. The time required for 10% of the amorphous NTR to crystallize (t_{90}) was estimated as an indicator of the crystallization tendency. The time-profiles of $x(t)$ were analyzed according to the Avrami equation (Eq. (2), $n = 3$) to calculate t_{90}:

$$x(t) = \exp[-kt^n] \tag{2}$$

where k is the crystallization rate constant and n is the Avrami index. HPLC analysis of stored NTR samples showed no evidence of degradation during melt-quenching and subsequent storage.

2.3. Determination of nucleation rate and crystal growth rate of NTR enantiomer

The nucleation rate and the crystal growth rate were determined for samples prepared in a space between two glass disks separated by a stainless steel ring. The NTR enantiomer–polymer mixture, which was described above, or the crystalline NTR enantiomer (1.5–2 mg) was placed on a clean glass disk (thickness: 0.12 mm, diameter: 16 mm) and heated at 180 °C in the DSC with a stainless steel ring (inner diameter: 6 mm, thickness: 20 μm) as a spacer. After the sample had melted completely, it was covered with another glass disk (thickness: 0.12 mm, diameter: 12 mm) to yield an amorphous layer between the glasses. Attention was paid to ensure that the layer was free of bubbles. For measurements at temperatures above 40 °C, the sample was stored in the chamber of a heating/cooling stage for microscopy (THMS600, Linkam Scientific Instruments), which had been adjusted to a prescribed temperature in advance. The moisture in the chamber was removed by purging with dry nitrogen gas for 10–15 min. Microscopic images of the sample were recorded at appropriate time intervals by a digital camera (DXM1200F, Nikon Corporation) attached to a polarized light microscope (ECLIPSE E600 POL, Nikon Corporation) with a 10× objective lens. In order to minimize possible photo degradation of NTR by the polarized light, the light source of the microscope was shut off when images were not recorded. For measurements at 30 °C, the samples were stored at 30 °C in desiccators containing phosphorous pentoxide. After an appropriate period of storage, microscopic images of the sample were recorded, and the sample was again stored at 30 °C in a dry state.

2.3.1. Measurement of nucleation rate

The nucleation rate of the NTR enantiomers was estimated from time-profiles of nucleation site density determined from microscopic images of the stored samples. Nucleation site density per unit volume was calculated from the number of nucleation sites per unit area and the depth of field of the lens used for data collection. The depth of field was calculated to be 8.46 μm from the wavelength of the light (546 nm) and the numerical aperture of the lens (0.25). For samples with more than a dozen nucleation sites per fixed field at the end of the observation period, nucleation sites were counted in one fixed field. For samples with less than a dozen nucleation sites per field near the end of the observation period, and those stored at 30 °C, nucleation sites were counted for 12 individual areas in one sample, and the average value from the 12 individual images was regarded as the number of nucleation sites per field. The nucleation rate was obtained from the slope of time-profiles of the number of nucleation sites per unit volume (nucleation site density) at steady state. In cases showing preferential nucleation and growth at the sample periphery, these sites were not included in the analysis. The reported nucleation rates were average values of those obtained for at least three samples prepared separately.

2.3.2. Measurement of crystal growth rate

The crystal growth rates at temperatures above 40 °C were measured concurrently with the nucleation rate measurements as described above. The measurements at 30 °C were carried out using samples that showed more than a dozen nucleation sites per one field after a few months of storage in desiccators containing phosphorous pentoxide. The sample was placed in the chamber of the heating/cooling stage controlled at 30 °C, and the growth of crystals was observed in a fixed field. The radius of each crystal was estimated from a circular approximation by using Lumina Vision software (Mitani Co.). The average crystal growth rate was calculated from the increase in the radius as a function of time based on observations of at least 20 crystals.

2.4. FT-IR

FI-IR spectra were collected using a FT/IR-6300 (JASCO Corporation) by the KBr method at ambient room temperature. Transmission spectra were obtained for KBr disks containing 1–1.5% sample at a resolution of 0.4 cm^{-1} within the range of 4000–400 cm^{-1}. An accumulation of 128–256 scans was acquired for each disk.

3. Results

3.1. Effects of polymers on the overall crystallization rates of NTR enantiomers in solid dispersions

No significant differences in the melting point (158 °C), T_g (33 °C) and ΔC_p at T_g (0.40 J/g/K) were observed between (−)-NTR and (+)-NTR. Table 1 shows the T_g values of amorphous solid dispersions of (−)-NTR and (+)-NTR. There appeared to be no significant difference in the T_g values between the two. The solid dispersions containing HPMC (10–20%) and 5% PVP showed T_g values similar to that of each NTR enantiomer alone. T_g values for solid dispersions containing 10% PVP were slightly higher than that of each NTR enantiomer alone, whereas solid dispersions containing HPMCP (10–20%) exhibited T_g values slightly lower than that of each NTR enantiomer alone.

Fig. 2 shows time-profiles of overall crystallization of NTR enantiomers at 60 °C. No significant differences in the overall crystallization profiles were observed between (−)-NTR and (+)-NTR without polymer (Fig. 2(a)), and between (−)-NTR and (+)-NTR in solid dispersions containing 10% PVP (Fig. 2(b)). In contrast, differences in time-profiles between the enantiomers were observed for solid dispersions containing 10% HPMC or HPMCP: (+)-NTR crystallized more slowly than (−)-NTR, as shown in Fig. 2(c) and (d). Table 2 shows the t_{90} values for the amorphous NTR enantiomers obtained for NTR alone and NTR in the solid dispersions. The t_{90} values for (−)-NTR without polymer and those of solid dispersions containing 5–10% PVP were almost the same as the t_{90} values for (+)-NTR without polymer and those of solid dispersions containing 5–10% PVP, respectively, at the temperatures studied. The t_{90} values at 50 and 60 °C for (+)-NTR were 1.5–2.0 times longer than that for (−)-NTR in solid dispersions containing 10–20% HPMC or HPMCP. At 40 °C, however, any difference between the enantiomers was not clear.

Table 1
T_g of pure NTR enantiomers and their solid dispersions with a polymer.

Polymer	Polymer content [%]	T_g[a] [°C]	
		(−)-NTR	(+)-NTR
None	0	33.2 ± 0.1	33.1 ± 0.2
HPMC	10	33.1 ± 1.0	33.0 ± 0.7
	20	33.1 ± 0.8	33.0 ± 0.7
HPMCP	10	31.2 ± 0.7	31.0 ± 0.4
	20	30.8 ± 1.2	30.5 ± 0.9
PVP	5	33.0 ± 0.2	33.1 ± 0.2
	10	36.3 ± 1.2	36.2 ± 0.8

[a] Average ± standard deviation (n = 3).

3.2. Effects of polymers on the nucleation rate and crystal growth rate

Fig. 3 shows the typical micrographs of NTR crystals grown from amorphous pure enantiomers and their solid dispersions with a polymer. The recrystallized NTR enantiomers without polymers showed a melting point of 158 °C, suggesting the same crystal form as the originally resolved stable one. The melting point of the samples containing 10% HPMC, HPMCP and PVP was approximately 151 °C in all cases, regardless of the various crystal shapes shown in Fig. 3. The difference from the melting point of the pure enantiomers would have been due to melting point depression by the

Table 2
t_{90} for NTR enantiomers with and without polymer.

Temperature [°C]	Polymer	[%]	t_{90}[a] [h]			
			(−)-NTR		(+)-NTR	
40	None	0	41	(1)	41	(1)
	HPMC	10	230, 240[b]		230, 230[b]	
	HPMCP	10	49	(1)	49	(1)
50	None	0	5.7	(0.2)	5.7	(0.1)
	PVP	10	250	(10)	240	(4)
	HPMC	10	17	(0.4)	25	(0.1)
	HPMCP	10	6.1	(0.3)	11	(0.3)
60	None	0	1.1	(0.1)	1.1	(0.1)
	PVP	5	3.5	(0.1)	3.6	(0.1)
		10	25 ± 3[c]		25 ± 3[c]	
	HPMC	10	3.8, 4.1[b]		6.7, 6.9[b]	
		20	8.7	(0.3)	15	(0.4)
	HPMCP	10	1.5 ± 0.2[c]		2.7 ± 0.3[c]	
		20	3.2	(0.1)	6.4	(0.2)

[a] The values in parentheses are standard error estimated from single experiments using Origin 8.1 software (Lightstone Corp.).
[b] Results with two values represent the results obtained from duplicate experiments using separately prepared samples.
[c] Mean ± standard deviation (n = 3).

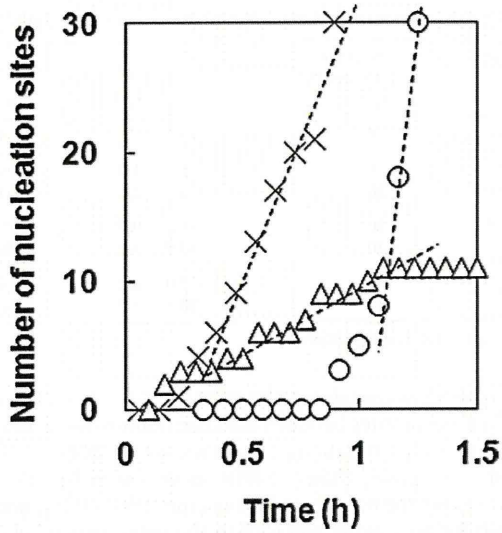

Fig. 4. Time profiles of the number of nucleation sites per field of view for (+)-NTR at 50 °C (○), 60 °C (×) and 70 °C (△). The dotted lines show the linear regression at steady state.

added polymers, as the melting point fell gradually with increasing polymer content (data not shown). The data suggested that differences in crystal habit, rather than polymorphism, might have been responsible for the differences in crystal shape among the solid dispersions.

Fig. 4 shows the typical time-profiles of the nucleation of amorphous NTR enantiomer stored at various temperatures. The lower the storage temperature, the longer the period required before the first crystal was observed. The nucleation rates at steady state were obtained from the slope of the lines in Fig. 4, and these were plotted against storage temperature (Fig. 5). As expected from the similar overall crystallization profiles of the NTR enantiomers (Fig. 2(a) and (b)), no significant difference in the nucleation rates between (−)-NTR and (+)-NTR was observed for amorphous NTR alone and the solid dispersions containing PVP within the temperature range studied (Fig. 5(a)). In contrast, the nucleation rates of (+)-NTR were lower than those of (−)-NTR in the solid dispersions containing HPMC and HPMCP (Fig. 5(b)) within the temperature range of 50–70 °C. At 40 °C, however, the differences in the rates between (−)-NTR and (+)-NTR were not pronounced. These results were consistent with the t_{90} values of the enantiomers shown in Table 2.

Fig. 6 shows the typical time-profiles of the NTR crystal growth at 60 °C. Crystal radius increased linearly with time, and the growth rate was estimated from linear regression of the plots. The higher the temperature, the faster the crystals grew within the temperature range studied (Fig. 7). In contrast to the nucleation rates, no significant growth rate differences between the NTR enantiomers were observed, irrespective of the absence or presence of any polymer.

3.3. FT-IR

FT-IR spectra (4000–400 cm^{-1}) of (−)-NTR and (+)-NTR were indistinguishable from one another for both the amorphous and the crystalline forms. Similarly, the FT-IR spectra of amorphous solid dispersions were almost the same for (−)-NTR and (+)-NTR with any polymer. Fig. 8 shows the spectra for crystalline (−)-NTR (dotted line in Fig. 8 (a)), NTR solid dispersions containing 25–75% HPMC and HPMC alone (dotted line in Fig. 8 (c)) in the range of 1800–1550 cm^{-1}, corresponding to C=O stretching region of NTR. Spectra with and without an asterisk represent that of (−)-NTR

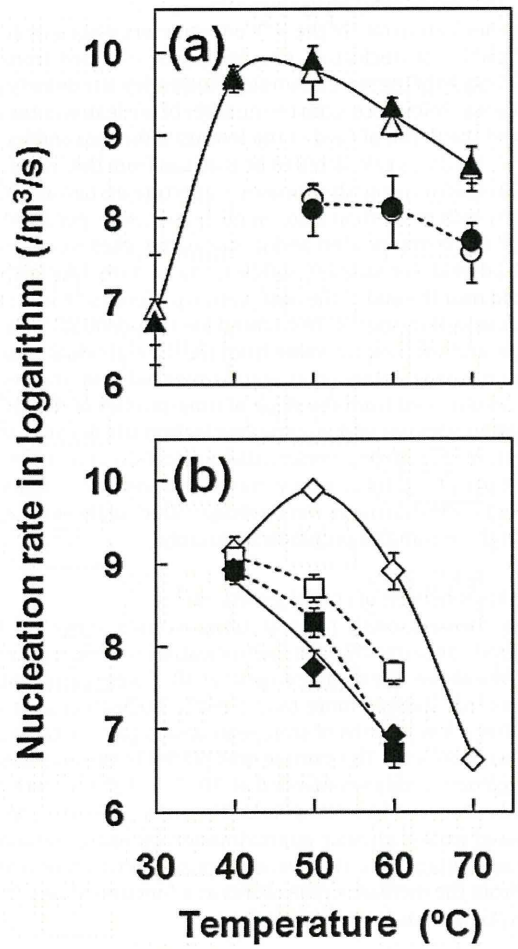

Fig. 5. Plots of nucleation rate as a function of temperature. Error bars represent standard deviation for at least triplicate experiments. (a) △, ▲: without polymer, ○, ●: 10% PVP and (b) □, ■: 10% HPMC, ◇, ♦: 10% HPMCP. Open symbols represent (−)-NTR and solid symbols represent (+)-NTR.

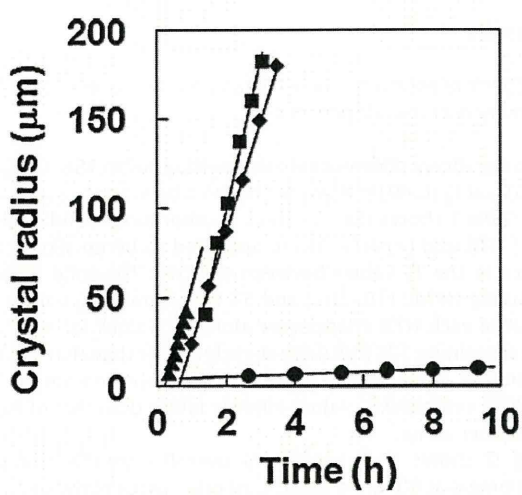

Fig. 6. Typical time profiles of the radius of NTR crystals in (+)-NTR alone (▲), and solid dispersions with 10% HPMC (■), 10% HPMCP (♦) and 10% PVP (●) at 60 °C.

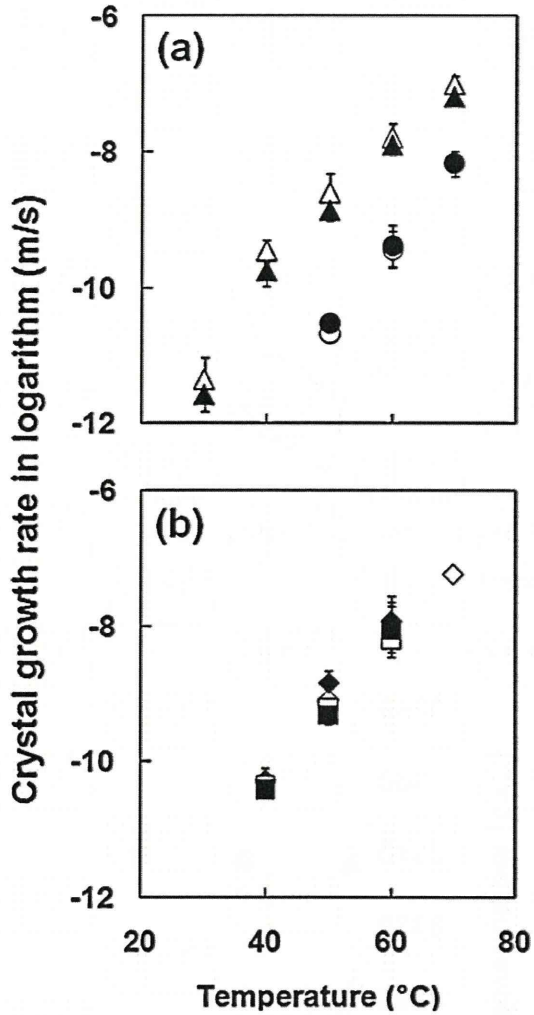

Fig. 7. Temperature dependence of crystal growth rate of NTR enantiomers. Error bars represent standard deviation for at least triplicate experiments. (a) △, ▲: without polymer; ○, ●: 10% PVP and (b) □, ■: 10% HPMC; ◇, ♦: 10% HPMCP. Open symbols represent (−)-NTR and solid symbols represent (+)-NTR.

and (+)-NTR, respectively. Despite its vicinity to the asymmetric carbon, carbonyl group of (−)-NTR and (+)-NTR showed same spectra even in the presence of HPMC. Likewise, no difference in spectra between solid dispersions of (−)-NTR and (+)-NTR containing HPMCP was observed (data not shown).

Fig. 9 shows the spectra in the range of 3650–3150 cm^{-1}, corresponding to NH stretching vibrations of nifedipine derivatives (Konno and Taylor, 2006), where the changes in peak position were obvious upon mixing with polymers as solid dispersions. There were also no obvious differences in the spectra between the two enantiomers. The peak around 3350 cm^{-1} was assigned to the NH stretching vibration that was expected to be involved in the hydrogen bonding between the drug and a polymer. The peak position was shifted from 3360 cm^{-1} to 3337 cm^{-1} by amorphization, and additionally shifted to 3291 cm^{-1} in the presence of 50% PVP (Figs. 9(b) and 10). On the other hand, for solid dispersions prepared with HPMC and HPMCP, the peak position showed a degree of shift to a higher wavenumber (Figs. 9(c) and (d) and 10). The peak position for solid dispersions with 75% HPMCP was nearly equal to that of the pure NTR crystals. These changes in peak position showed the same tendency for both (+)-NTR and (−)-NTR.

4. Discussion

The overall crystallization of (−)-NTR proceeded faster than that of (+)-NTR in solid dispersions with HPMC or HPMCP (Fig. 2(c) and (d)), while that for solid dispersions with PVP proceeded at almost the same rate, regardless of NTR chirality (Fig. 2(b)). The nucleation rates of (−)-NTR were greater than those of (+)-NTR in solid dispersions with HPMC or HPMCP at 50–70 °C (Fig. 5(b)), while no difference in nucleation rates between the NTR enantiomers was observed for solid dispersions with PVP (Fig. 5(a)). The T_g values for samples using (−)-NTR or (+)-NTR were almost the same (Table 1), suggesting that the differences in the overall crystallization profiles and nucleation rates between the enantiomers are not due to differences in molecular mobility between (−)-NTR and (+)-NTR in solid dispersions with HPMC or HPMCP. The difference in physical stability between the two enantiomers may be explained by the difference in strength of NTR–polymer interaction between them. The results obtained from FT-IR measurements indicate that PVP interacts with NTR through hydrogen bonding at the NH moiety of NTR (Figs. 9 and 10). Almost the same degrees of shift in wavenumber for NH stretching suggest a similar strength of hydrogen bond interaction for (−)-NTR and (+)-NTR. PVP polymer chains possess an asymmetric carbon in a monomer unit, and are composed of monomer units with an equal ratio of R and S configurations. Therefore, (−)-NTR and (+)-NTR are considered to interact with PVP through hydrogen bonds of the same strength and number, resulting in a similar degree of physical stability between (−)-NTR and (+)-NTR. In contrast, HPMC and HPMCP are cellulose derivatives that are polymers of optically active D-glucose, and thus are expected to interact differently (strength and/or number) with NTR enantiomers, resulting in the difference in physical stability between (−)-NTR and (+)-NTR, although differences in interaction were not detectable by FT-IR. At 40 °C, however, the differences in physical stability between the enantiomers with HPMC or HPMCP were not remarkable (Table 2, Fig. 5). We do not have a satisfactory explanation for the loss of the difference in stabilization by HPMC and HPMCP. However, one possible explanation is as follows: The temperature dependence of the nucleation rate exhibits a maximum just above T_g because the nucleation rate is influenced by both molecular mobility and thermodynamic factors; an increase of temperature increases the molecular mobility, and thus the nucleation rate, whereas nucleation is thermodynamically favored at lower temperatures. A barrier due to molecular mobility is considered to play a predominant role in nucleation within the temperature range below the maximum point (Hancock and Zografi, 1997; Andronis and Zografi, 2000). Therefore, loss of the difference in physical stability between the enantiomers at 40 °C may be due to the predominant contribution of molecular mobility, since the molecular mobility is suggested to be similar for (−)-NTR and (+)-NTR in solid dispersions, as indicated by the T_g values (Table 1). However, physical stability data at temperatures below 40 °C, which are difficult to obtain within the commonly used experimental time scale, are needed in order to support this speculation.

In contrast to the nucleation rates, no significant difference in the crystal growth rates between the NTR enantiomers was observed for solid dispersions with HPMC or HPMCP (Fig. 7). The crystal growth rates for solid dispersions with HPMC or HPMCP were similar to those for each NTR enantiomer alone, indicating that the effects of HPMC and HPMCP on the crystal growth rate were small. This might be one of the reasons why differences in the crystal growth rate between the NTR enantiomers could not be detected in solid dispersions with HPMC or HPMCP.

It may be worth to note that PVP decreased the crystal growth rate of NTR enantiomers more than HPMC and HPMCP at all the temperatures studied (Fig. 7). On the other hand, PVP did not always decrease the nucleation rate of NTR more effectively than HPMC or